

## Fast Kicker for High Current Beam Manipulation in Large Aperture

V. Gambaryan<sup>1</sup> and A. Starostenko<sup>1,2</sup>

<sup>1</sup>Budker Institute of Nuclear Physics SB RAS, Novosibirsk, Russia

<sup>2</sup>Novosibirsk State University, Novosibirsk, Russia

### Abstract

The pulsed deflecting magnet (kicker) project was worked out in Budker Institute of Nuclear Physics. The kicker design parameters are: impulsive force, 1 mT\*m; pulse edge, 5 ns; impulse duration, 200 ns. The unconventional approach is that the plates must be replaced by a set of cylinders. The obtained magnet construction enables the field homogeneity to be controlled by changing current magnitudes in cylinders. Furthermore, we demonstrated the method of field optimization. In addition, measurement technique for the harmonic components was considered and the possibility of control harmonic components value was demonstrated.

### Keywords

Kicker; impulse magnet; high current beam; field harmonic components.

## 1 Kicker actual design

Taking into account results obtained previously [1] at the Budker Institute of Nuclear Physics (BINP) a kicker prototype was developed. The magnet cross-section is shown in Fig. 1. The physical magnet length is  $\approx 650$  mm. The magnet aperture is 100 mm. The vacuum chamber diameter and the conductor cylinder diameter are 164 mm and 28 mm, respectively. The cylinders are made of steel, as is the body of the magnet. The ceramic feedthroughs were also developed at BINP.

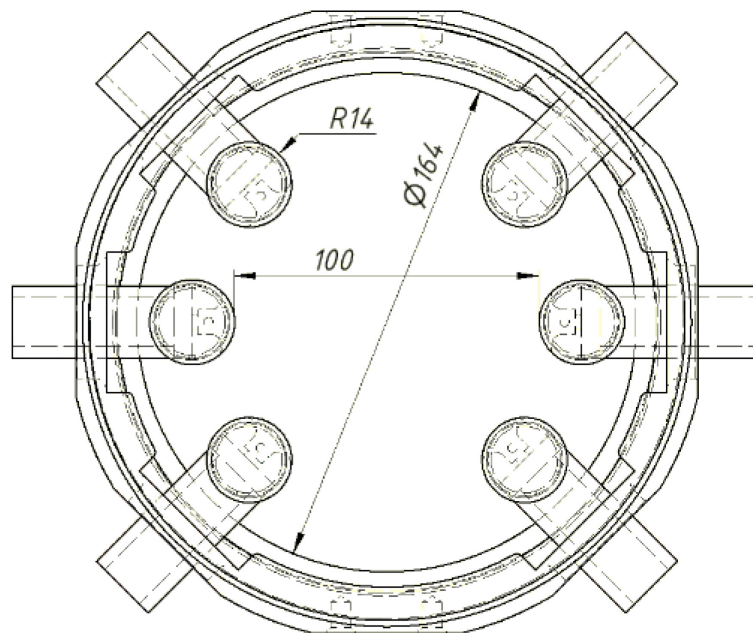


Fig. 1: Kicker actual design (all dimensions are in mm)

## 2 Magnetic field measurements

### 2.1 Experimental stand description

The experimental stand, shown in Fig. 2, consists of the following parts:

1. kicker;
2. pulse generator;
3. induction coil magnetometer;
4. VSDC2—precision digital signal integrators with accurate synchronization [2];
5. hand caliper;
6. step motors with controllers;
7. PC with specialized software.

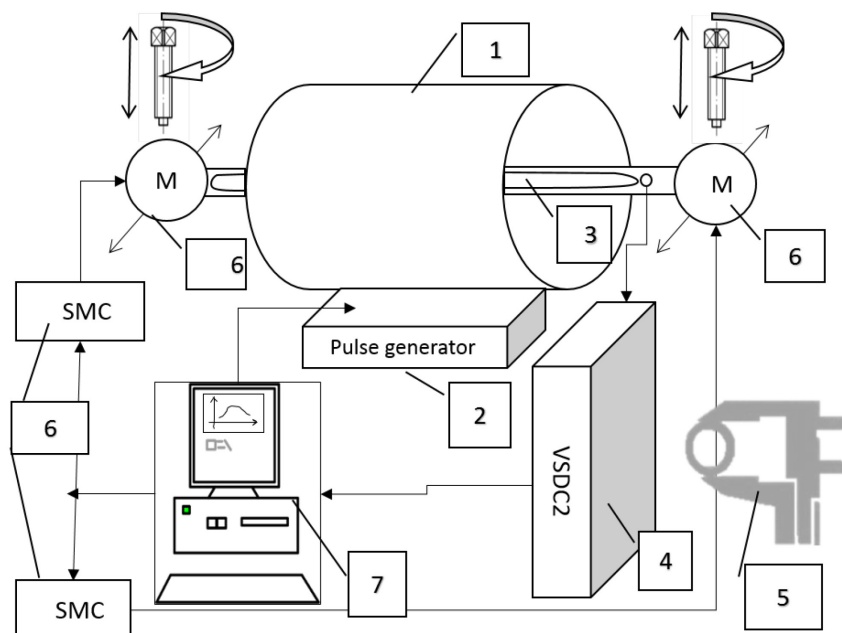


**Fig. 2:** Principal scheme of magnetic field measurement stand: 1, kicker; 2, pulse generator; 3, induction coil magnetometer; 4, VSDC2; 5, hand caliper; 6, step motors with controllers; 7, PC with specialized software; M, motor; SMC, step motor controller.

The kicker is fixed on a metal frame. Step motors provide movement in the horizontal plane. The vertical displacement of step motors is realized only by hand-turned screws. For both step motors, the vertical position must be controlled using a hand caliper. All of the stand components were precisely aligned with the help of the BINP Geodesy group.

### 2.2 Power pulse generator

The generator provides the following current characteristics: maximum frequency, 12.5 kHz; maximum current, 200 A.

At this stage in our research, we have a switching power supply that does not fully comply with our requirements. The final prototype bandwidth should be about 200 MHz. Therefore, we need to determine how precisely we can measure the magnetic field using a low frequency power supply.

A magnetic field distribution with frequency values ranging from 12.5 kHz to 1 MHz was simulated using finite element method magnetics (FEMM) [3] (see Fig. 3(a)). We need to compare the form of field dependence curves obtained. We calculate the percentage difference between the minimum and maximum values of each curve, normalized to the 1 MHz curve. Figure 3(b) demonstrates a decrease in discrepancy with increasing frequency. The discrepancy level in our case (12.5 kHz) is  $\approx 4\%$ . This result allows us to assume that our measurements are acceptable.

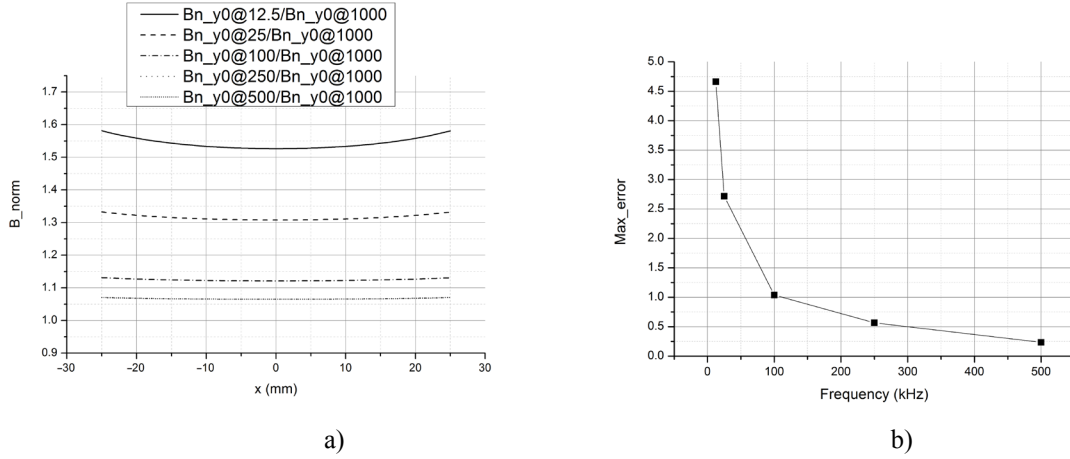


**Fig. 3:** (a) Magnetic field distribution versus position in central plane for different frequencies; (b) error level for different frequencies.

### 2.3 Induction coil magnetometer

The induction coil consists of five wire turns ( $N = 5$ ). It has width  $w = 5$  mm and length  $l = 1000$  mm. The wire diameter is 0.2 mm. The coil base is made of fiberglass plastic strip. The induction coil principle is derived directly from Faraday's law:

$$E(t) = -\frac{d\Phi_B(t)}{dt}, \quad (1)$$

where  $E$  is the electromotive force (EMF) and  $\Phi_B$  is the magnetic flux. Time integration of the EMF gives the magnetic flux. From the magnetic flux definition, we can determine the maximal magnetic field value:

$$B_{max} = \frac{-\int_0^{T_0} E(t) dt}{N \cdot w \cdot l}, \quad (2)$$

where  $T_0$  is the integration time chosen such to provide a maximum integral value,  $N$  is the number of coil turns, and  $w$  and  $l$  are the coil width and length, respectively.

For example, Fig. 4 shows typical signals. The first channel (grey dashed curve) is a signal from the coil and the second channel (black curve) is a current monitor signal.

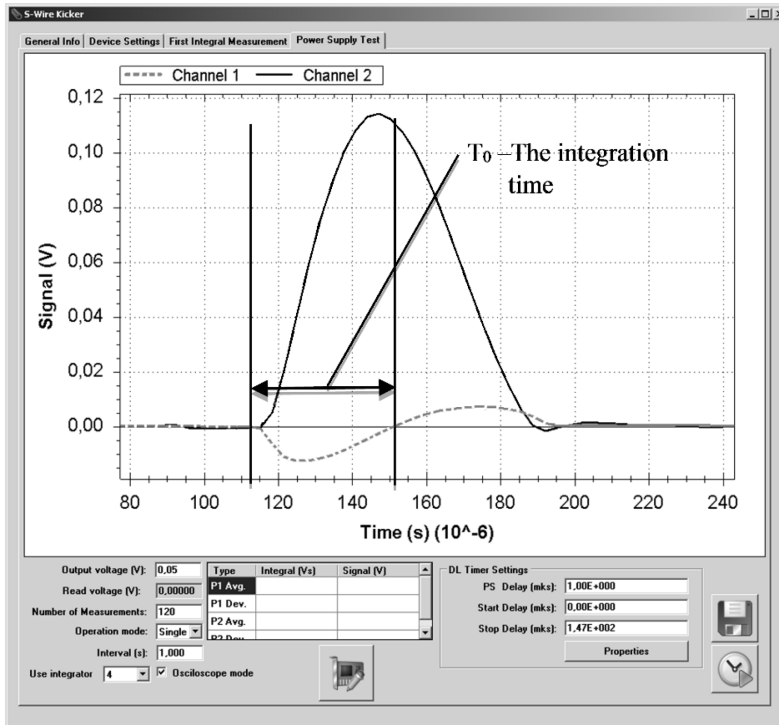


Fig. 4: Typical signals: Channel 1, signal from magnetometer; Channel 2, signal from current wave form

We supply the coil signal to VSDC2. Software ‘S-Wire Kicker’ created at BINP is integrated in the experimental stand. The program can control the step motors and pulse generator and store the measurements on a hard disk drive.

The magnetic field distribution was measured in the central part of the kicker. The area investigated is almost  $2 \times 2$  cm square. Measurements were carried out at five vertical positions:  $-2$  cm,  $-1$  cm,  $0$  cm,  $1$  cm, and  $2$  cm. The horizontal shift was automatically realized using the ‘S-Wire Kicker’ program within the range  $-1.8$  cm to  $1.8$  cm, in increments of  $0.1$  cm. Five measurements were made at each point, and the average taken. The obtained values were used to form a magnetic field distribution map. To compare experimental results with calculations, we simulated the FEMM task with the same current value obtained from the current monitor.

### 3 Magnetic field measurements

To measure the magnetic field distribution in the experiment, we used a single generator. The cable commutation scheme is shown in Fig 5.

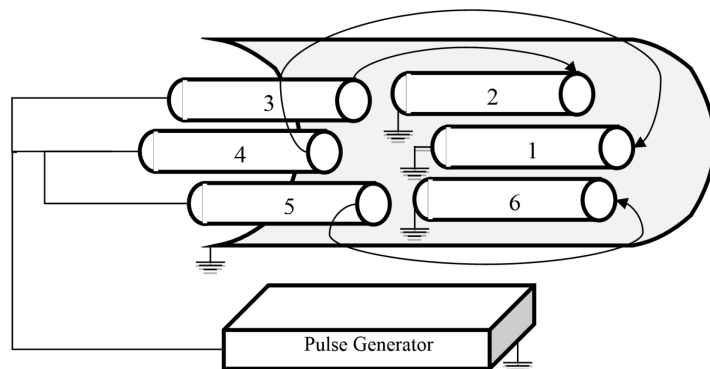
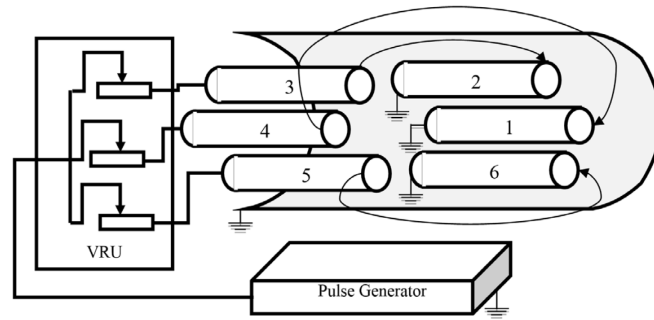


Fig. 5: Kicker commutation

A variable resistance unit was made with the aim of controlling a current in the separate cylinders. The commutation scheme with variable resistance unit is shown in Fig. 6. Using this scheme, an improved magnetic field distribution can be obtained.



**Fig. 6:** Kicker commutation diagram with variable resistance unit (VRU)

### 3.1 Experimental results

In this part, we present the results of the magnetic field measurements. The experimental data in comparison with results calculated using FEMM are shown in Figs. 7 and 8 ((a) experimental; (b) calculation using FEMM).

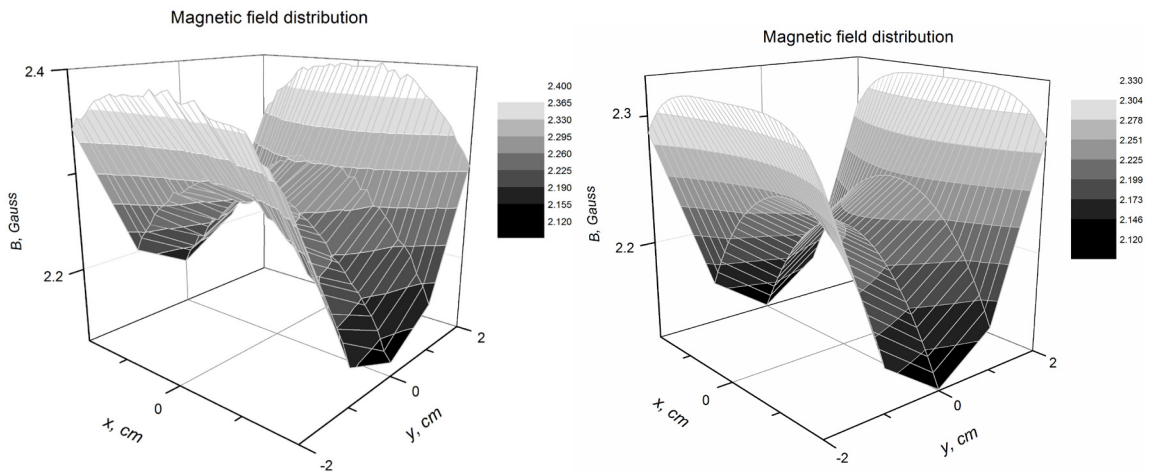


**Fig. 7:** Magnetic field distribution: (a) measured; (b) calculated

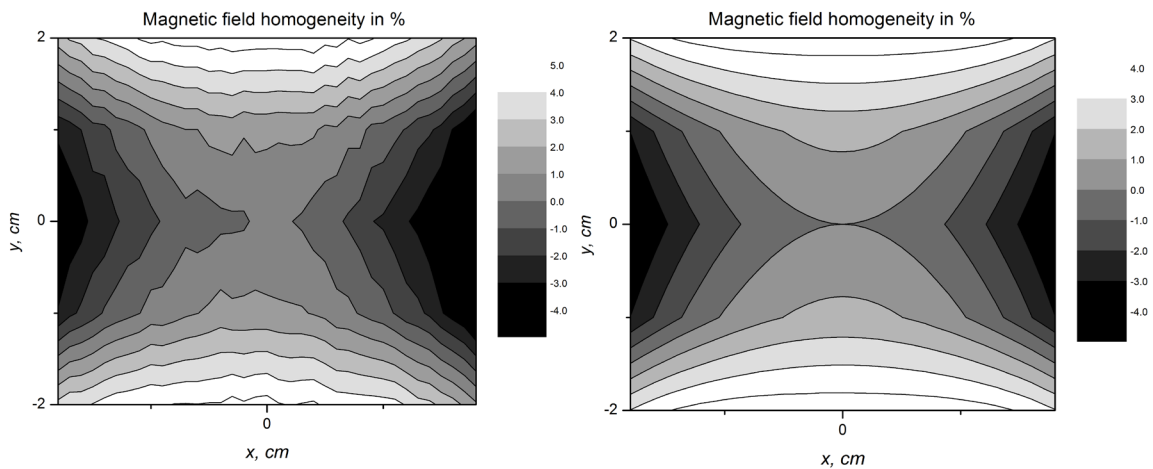


**Fig. 8:** Magnetic field homogeneity: (a) measured; (b) calculated

We can see that the measurements agree with the simulation to sufficient accuracy.

We have an opportunity of controlling the magnetic field distribution and homogeneity. To implement this, we need to set the specific current values in each conductor. The parametric optimization simulation was achieved in FEMM. We consider the upper and lower conductor currents to be  $I_0$  A. The current in the central conductor is  $k \cdot I_0$  A, where  $k$  is the optimizing parameter:

$$I_2 = I_6 = -I_3 = -I_5 = I_0, \quad I_1 = -I_4 = k \cdot I_0.$$

The optimization goal is to minimize  $\Delta B$ , the field quality indicator:

$$\Delta B = \frac{B_{\max} - B_{\min}}{B_{\min}} \cdot 100\% . \quad (3)$$

The dependence of the magnetic field quality on the parameter  $k$  is shown in Fig. 9. As a result of the optimization, we obtain the following ratio: the first and fourth currents must be 1.5 times larger than the others, i.e.  $k = 1.5$ .

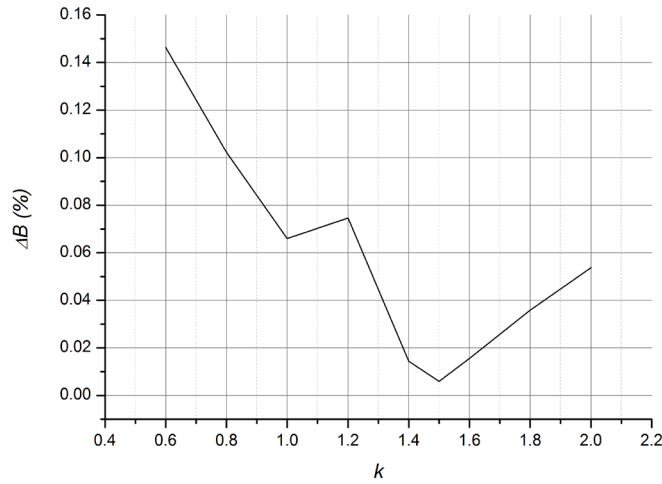


Fig. 9: Magnetic field quality as a function of current ratio

Using the variable resistance unit, the current in each conductor was tuned in accordance with the optimization results and the measurement was repeated. The results obtained are shown in Figs. 10 and 11.

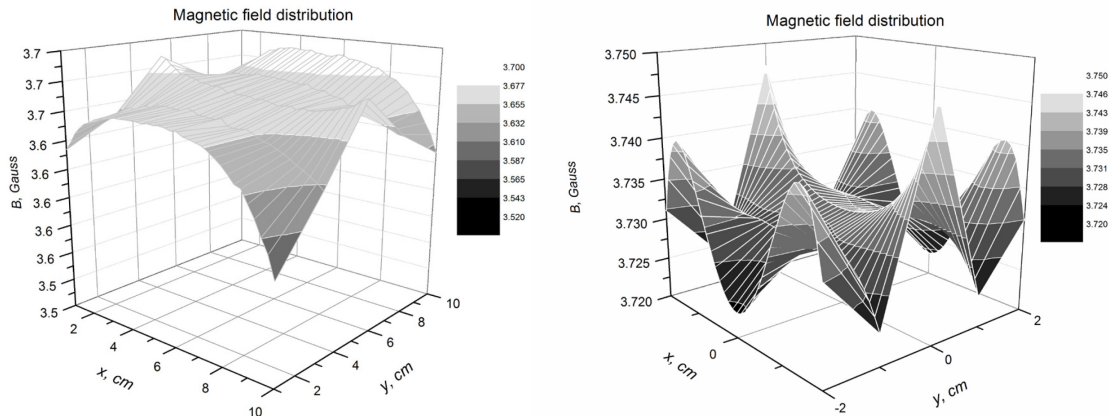
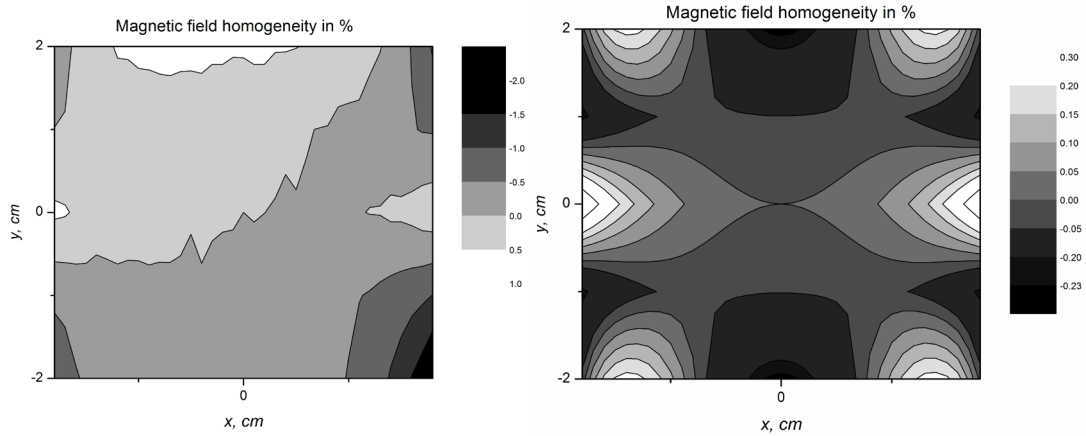


Fig. 10: Magnetic field distribution after current correction using variable resistance unit: (a) measured; (b) calculated.



**Fig. 11:** Magnetic field homogeneity after current correction using variable resistance unit: (a) measured; (b) calculated.

The magnetic field measured experimentally turned out to be asymmetric. However, we see that the homogeneity value is close to the calculated one. The reason for this asymmetry is not completely explored. We have considered a number of assumptions, but they need to be checked. One of these is the limited induction coil magnetometer accuracy and another is that there may be some imperfections in the electrical contacts. We plan to repeat the measurements to provide more accurate results.

#### 4 Field harmonics components

The chosen geometry allows us to use an interesting method of controlling the distribution of the magnetic field harmonics. Using FEMM, one can obtain the angular dependence of the normal and tangential components of the magnetic field along the circumference (see Fig. 12(a)). This dependence for an ideal dipole field is sinusoidal (see Fig. 12(b)). The field harmonics expansion allows us to judge how close to an ideal field such a field is.

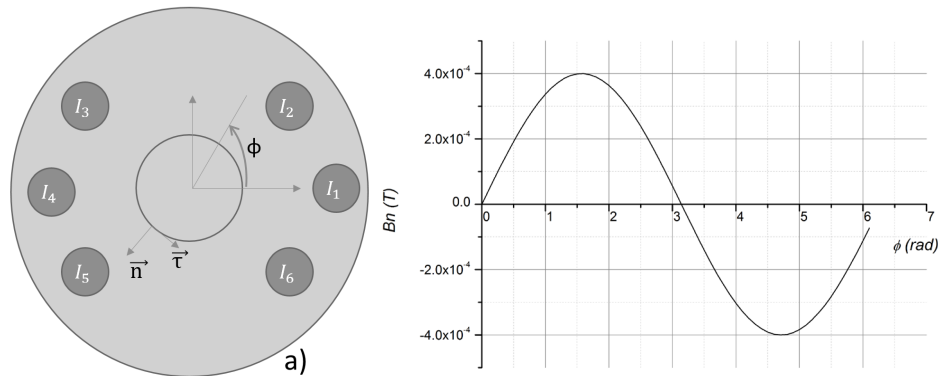


**Fig. 12:** Magnetic field along circumference: (a) magnet layout; (b) sinusoidal magnetic field signal

The normal and tangential magnetic field component functions can be expanded in a sine series (Eqs. 4 and 5). The coefficients of such series are harmonic components. The first coefficient is a dipole component, the second is a quadruple component, and so on.

$$B_n(\varphi) = B_{1n} \sin(\varphi) + B_{2n} \sin(2\varphi) + B_{3n} \sin(3\varphi) + B_{4n} \sin(4\varphi) + \dots \quad (4)$$

$$B_\tau(\varphi) = B_{1\tau} \sin(\varphi) + B_{2\tau} \sin(2\varphi) + B_{3\tau} \sin(3\varphi) + B_{4\tau} \sin(4\varphi) + \dots \quad (5)$$

For example, the harmonic components for an optimal current distribution case are shown in Fig. 13. As expected, all harmonics are extremely small except the first one. It is worth noting that the third and fifth components have different signs.

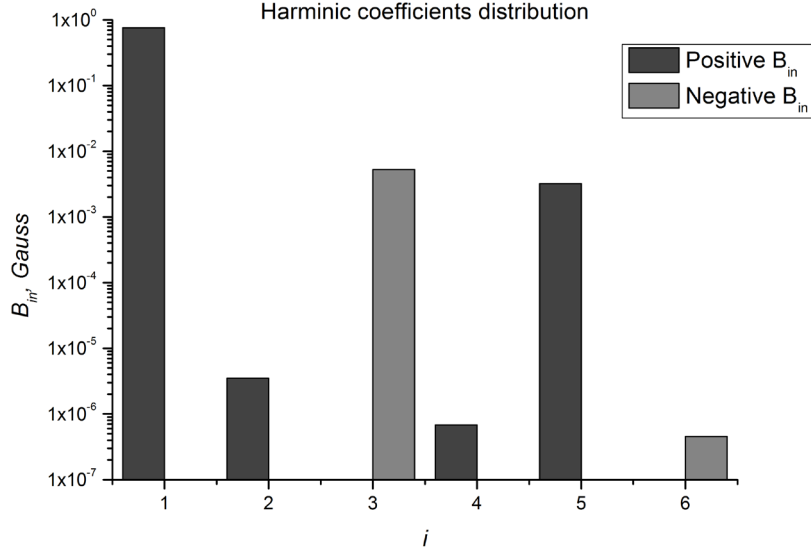


**Fig. 13:** Harmonic field component distribution in logarithmic scale

Owing to the presence of separated conductors, we can obtain the matrix of coefficients describing the dependence of harmonics changes on current changes in each conductor—a harmonics response matrix. This matrix was calculated:

$$K_n = \begin{pmatrix} K_{1,1} & \dots & K_{1,6} \\ \dots & \dots & \dots \\ K_{6,1} & \dots & K_{6,6} \end{pmatrix} = \begin{pmatrix} -1.28 \times 10^{-3} & -9.30 \times 10^{-4} & 9.30 \times 10^{-4} & 1.28 \times 10^{-3} & 9.30 \times 10^{-4} & -9.30 \times 10^{-4} \\ -6.73 \times 10^{-4} & 1.12 \times 10^{-4} & 1.12 \times 10^{-4} & -6.73 \times 10^{-4} & 1.12 \times 10^{-4} & 1.12 \times 10^{-4} \\ -3.05 \times 10^{-4} & 2.42 \times 10^{-4} & -2.42 \times 10^{-4} & 3.05 \times 10^{-4} & -2.42 \times 10^{-4} & 2.42 \times 10^{-4} \\ -1.31 \times 10^{-4} & 9.96 \times 10^{-5} & 9.96 \times 10^{-5} & -1.31 \times 10^{-4} & 9.96 \times 10^{-5} & 9.96 \times 10^{-5} \\ -4.52 \times 10^{-5} & 2.59 \times 10^{-5} & -2.59 \times 10^{-5} & 4.52 \times 10^{-5} & -2.59 \times 10^{-5} & 2.59 \times 10^{-5} \\ -1.30 \times 10^{-5} & 2.72 \times 10^{-6} & 2.71 \times 10^{-6} & -1.30 \times 10^{-5} & 2.73 \times 10^{-6} & 2.71 \times 10^{-6} \end{pmatrix}. \quad (6)$$

From the simulation results, we have a set of harmonics (see Fig. 13). This can be presented as a vector:

$$\vec{B}_{n0} = \begin{pmatrix} B_{1n0} \\ \dots \\ B_{6n0} \end{pmatrix} = \begin{pmatrix} 7.56 \times 10^{-1} \\ 3.52 \times 10^{-6} \\ -5.26 \times 10^{-3} \\ 6.81 \times 10^{-7} \\ 3.21 \times 10^{-3} \\ -4.55 \times 10^{-7} \end{pmatrix}. \quad (7)$$

We consider  $\vec{B}_{n0}$  as optimal. The experimentally measured set of harmonics is likely to be different from the optimal. To correct it, we need to add corrections to the currents. The current deviation vector can be obtained by multiplying the inverse matrix  $K$  by a harmonic deviation vector:

$$\vec{\Delta I} = K_n^{-1} \vec{B}_n. \quad (8)$$

To verify this approach, we present the following calculations. For an optimal current distribution, we have a certain set of harmonics  $\overrightarrow{B_{n0}}$ . Calculations in FEMM with random changes in the current vector give us a new set of harmonics:

$$I' = I_0 + \begin{pmatrix} -0.1 \\ 0.2 \\ 0.1 \\ -0.15 \\ 0.11 \\ 0.2 \end{pmatrix}; \quad \overrightarrow{B_{n\_error}} = \begin{pmatrix} 7.56 \times 10^{-1} \\ 2.40 \times 10^{-4} \\ -5.22 \times 10^{-3} \\ 9.42 \times 10^{-5} \\ 3.21 \times 10^{-3} \\ 4.46 \times 10^{-6} \end{pmatrix}. \quad (9)$$

Then we calculate the harmonic deviation vector and multiply it by an inverse matrix. We get a vector, which is the optimum current deviation vector:

$$\overrightarrow{\Delta B_n} = \overrightarrow{B_{n\_error}} - \overrightarrow{B_{n0}} = \begin{pmatrix} -2.41 \times 10^{-4} \\ 2.37 \times 10^{-4} \\ 3.07 \times 10^{-5} \\ 9.35 \times 10^{-5} \\ 2.65 \times 10^{-6} \\ 4.91 \times 10^{-6} \end{pmatrix} \quad (10)$$

$$\overrightarrow{\Delta I} = K_n^{-1} \overrightarrow{B_n} = \begin{pmatrix} -0.1 \\ 0.076315 \\ 0.055879 \\ -0.15 \\ 0.154121 \\ 0.323674 \end{pmatrix}. \quad (11)$$

Then we subtract it from the current values of the current (Eq. 12), repeat the calculation using FEMM and check the harmonics (Eq. 13):

$$\overrightarrow{I''} = \overrightarrow{I'} - \overrightarrow{\Delta I} \quad (12)$$

$$\overrightarrow{B_{n1}} = \begin{pmatrix} 7.56 \times 10^{-1} \\ 3.51 \times 10^{-6} \\ -5.26 \times 10^{-3} \\ 6.82 \times 10^{-7} \\ 3.21 \times 10^{-3} \\ -4.23 \times 10^{-7} \end{pmatrix}. \quad (13)$$

The small difference between the new values of harmonics and the optimum shows the efficiency of the method. The harmonic vector has been corrected with a very good accuracy:

$$\vec{B}_{n1} - \vec{B}_{n0} = \begin{pmatrix} -3.29 \times 10^{-10} \\ -4.64 \times 10^{-9} \\ 2.12 \times 10^{-9} \\ 8.23 \times 10^{-10} \\ -1.09 \times 10^{-8} \\ 3.19 \times 10^{-8} \end{pmatrix}. \quad (14)$$

## 5 Summary

We carried out magnetic field measurements. For this purpose, a magnetic measurement stand was created and tested. The correction technique for harmonic components was theoretically verified. Our future aims are to carry out more precise measurements and to implement the magnetic field quality improvement procedure.

## References

- [1] V.V. Gambaryan and A.A. Starostenko, Fast kicker, Proc. 6th International Particle Accelerator Conf., Richmond, VA, 2015, paper MOPTY033, p. 1001.  
<https://jacowfs.jlab.org/conf/proceedings/IPAC2015/papers/mopty033.pdf>
- [2] A.M. Batrakov *et al.*, *Optoelectron. Instrum. Data Process.* **51** (2015) 51.  
<http://dx.doi.org/10.3103/S8756699015010082>
- [3] <http://www.femm.info>, last accessed September 10th 2016.